

Petrov-Galerkin flux upwinding for mixed mimetic spectral elements, and its application to vorticity stabilisation in shallow water

David Lee^{a,*}

^a*Department of Mechanical and Aerospace Engineering, Monash University, Melbourne 3800, Australia*

Abstract

Upwinded mass fluxes are described and analysed for advection operators discretised using mixed mimetic spectral elements. This involves a Petrov-Galerkin formulation by which the mass flux test functions are evaluated at downstream locations along velocity characteristics. As for the original operator, the upwinded mass flux advection operator is conservative, however unlike the original operator, which is purely hyperbolic, the upwinded operator adds dissipation which is biased towards high wave numbers. The upwinded operator also removes the spectral gaps present in the dispersion relation for the original operator. As for the original operator, a material form advection operator may be constructed by similarly downwinding the trial functions of the tracer gradients. Both methods allow for the recovery of exact energy conservation for an incompressible flow field via skew-symmetric formulations. However these skew-symmetric formulations are once again purely hyperbolic operators which do not suppress oscillations. Finally, the scheme is implemented within a shallow water code on the sphere in order to diagnose and interpolate the vorticity term. In the absence of other dissipation terms, it is shown to yield more coherent results for a standard test case of barotropic instability.

Keywords: Advection, Upwinding, Mimetic, Compatible, Mixed finite elements,

It is well known that in the absence of upwinding or diffusion, discrete approximations to hyperbolic terms result in spurious oscillations. Numerous methods have been devised to address this issue in the context of finite element methods, including the streamwise-upwind Petrov-Galerkin method [1] and variational multiscale methods [2]. These schemes have subsequently been applied within collocated spectral element discretisations [3]. In the present work we address this issue in the context of a mixed mimetic spectral element discretisation [4], a high order finite element method for which the $H(\text{div}, \Omega)$ function space of the mass flux is compatibly mapped to the $L^2(\Omega)$ space of the tracer field by the divergence operator [5].

Existing variational approaches to upwind stabilisation typically involve augmenting the test space with additional terms, for example a convective term that results in some form of symmetric positive definite operator which acts as a viscosity in the direction of the flow [1], or additionally a dual space in which the fine scales are represented via an adjoint problem from which the stabilisation terms are derived [2]. An alternative form of upwinding for mixed finite elements for Hamiltonian systems has been introduced whereby all of the test and trial functions in the $H(\text{div}, \Omega)$ space are projected onto upwind variants within the skew-symmetric operator so as to preserve energy conservation [6]. Here we instead base our methods around the idea of Lagrangian basis functions, which are evaluated at upstream locations in order to stabilise the resultant mass fluxes.

Mass conserving variational schemes based on Lagrangian basis functions have been developed previously for both finite element [7] and discontinuous Galerkin [8–10] methods. In each of the above cases the computation of fluxes via the extrusion of the test functions over the tracer field implies an adjoint problem in which the test functions are themselves advected along Lagrangian characteristics. In the present mixed finite element context, only the test functions for the mass fluxes are advected, and mass conservation is ensured since the trial functions, which compatibly map to the trial functions for the tracer via the divergence operator, remain static.

*Corresponding author. Tel. +61 452 262 804.
Email address: davelee2804@gmail.com (David Lee)

In the following section the advection problem is introduced for the standard mixed mimetic spectral element discretisation. In Section 2 variations on this method using upwinded test functions for flux form advection, or downwinded trial functions for material form advection will be described. Results for these new formulations, and comparisons to the original scheme will be presented in Section 3. As a practical demonstration of the Petrov-Galerkin upwind stabilisation, results are presented for the diagnosis and interpolation of vorticity for the rotating shallow water equations on the sphere in Section 4, and conclusions are discussed in Section 5.

1. Advection using mixed mimetic spectral elements

Consider the scalar advection equation of a tracer, q , subject to a velocity field, \mathbf{u} , expressed in conservative flux form as

$$\dot{q} + \nabla \cdot (\mathbf{u}q) = 0, \quad (1)$$

within a periodic spatial domain $\Omega = [0, L) \subset \mathbb{R}$, and a temporal coordinate $t = [0, \infty)$. We further assume the existence of two discrete, finite dimensional subspaces, $\mathcal{U}_h \subset H(\text{div}, \Omega)$ and $\mathcal{Q}_h \subset L^2(\Omega)$, such that \mathcal{Q}_h contains a set of functions which are square integrable, and \mathcal{U}_h contains a set of functions for which the sum of the functions and their divergence are square integrable. These spaces satisfy a compatibility property of the form

$$\mathcal{U}_h \xrightarrow{\nabla \cdot} \mathcal{Q}_h. \quad (2)$$

These two discrete subspaces are composed of a finite set of polynomial basis functions of degree p within each element such that

$$\mathcal{U}_h = \text{span}\{l_0^p(\xi), \dots, l_p^p(\xi)\}, \quad \mathcal{Q}_h = \text{span}\{e_0^p(\xi), \dots, e_{p-1}^p(\xi)\}, \quad (3)$$

where ξ is a local coordinate within the canonical element domain $[-1, 1] \subset \mathbb{R}$. For the remainder of this article, we will use as these subspaces the Lagrange polynomials of degree p with their roots as the Gauss-Lobatto-Legendre (GLL) points of equation degree, and the associated edge functions [4] respectively. These are given for the GLL nodes ξ_k as

$$l_i^p(\xi) = \prod_{\substack{k=0 \\ k \neq i}}^p \frac{\xi - \xi_k}{\xi_i - \xi_k}, \quad e_i^p(\xi) = - \sum_{k=0}^{p-1} \frac{dl_k^p(\xi)}{d\xi}. \quad (4)$$

The discrete mass flux, $\mathbf{F}_h \in \mathcal{U}_h$, and tracer field, $q_h \in \mathcal{Q}_h$ may be interpolated via the nodal and edge bases respectively as

$$\mathbf{F}_h(\xi) = \sum_{i=0}^p \hat{F}_i l_i^p(\xi), \quad q_h(\xi) = \sum_{i=0}^{p-1} \hat{q}_i e_i^p(\xi), \quad (5)$$

where \hat{F}_i and \hat{q}_i are the degrees of freedom. For the remainder of this article we will drop the superscripts, $l_i^p(\xi)$ and $e_i^p(\xi)$, and assume that p remains fixed at some specified degree for a given configuration.

Due to the orthogonality and compatibility properties of \mathcal{U}_h and \mathcal{Q}_h , by which the fundamental theorem of calculus is satisfied exactly between GLL (or any other choice of) nodes, the discrete divergence operator may be represented by a purely topological relation, known as an incidence matrix, and defined here over a periodic one dimensional domain as

$$\mathbf{E} = \begin{bmatrix} -1 & 1 & 0 & 0 & \dots & 0 \\ 0 & -1 & 1 & 0 & \dots & 0 \\ 0 & 0 & -1 & 1 & \dots & 0 \\ \vdots & \vdots & \vdots & \vdots & \ddots & \vdots \\ 1 & 0 & 0 & 0 & \dots & -1 \end{bmatrix}. \quad (6)$$

The discrete divergence of the mass flux onto a semi-discrete time derivative of the tracer field is then given in the strong form as

$$\dot{\hat{q}}_i = -\mathbf{E}_{ij} \hat{F}_j. \quad (7)$$

The mass flux is computed via a contraction of the tracer field onto the velocity field as

$$\langle l_i, l_j \rangle_{\Omega} \hat{F}_j = \langle l_i \cdot \mathbf{u}_h, e_k \rangle_{\Omega} \hat{q}_k, \quad \forall l_i \in \mathcal{U}_h, \quad (8)$$

where the brackets $\langle a, b \rangle_{\Omega} = \int \mathbf{a} \mathbf{b} d\Omega$ correspond to a bilinear operator, which may be integrated over each element as

$$\langle l_i, l_j \rangle = l_i(\xi_j) \cdot w_j |J(\xi_j)| \delta_{jk} \cdot l_m(\xi_k) \quad (9)$$

$$\langle e_i, e_j \rangle = e_i(\xi_j) |J(\xi_j)|^{-1} \cdot w_j |J(\xi_j)| \delta_{jk} \cdot |J(\xi_k)|^{-1} e_m(\xi_k), \quad (10)$$

where w_i are the weights and $|J(\xi_i)|$ are the Jacobian determinants for the i quadrature points, and δ_{ij} is the Kroeneker delta operator. The subscript Ω is added to denote the integration and assembly over all elements in the domain Ω . Note that the transformation for $l_i(\xi) \in \mathcal{U}_h$ to global coordinates is unity, while the transformation for $e_i(\xi) \in \mathcal{Q}_h$ is $J^{-1}(\xi)$. In higher dimensions these are transformed via the Piola mappings [11].

Equations (7) and (8) describe the semi-discrete integration of (1) [12, 13]. These may be expressed in a single equation as

$$\langle e_i, e_j \rangle_{\Omega} \hat{q}_j + \langle e_i, e_k \rangle_{\Omega} \mathbf{E}_{km} \langle l_n, l_m \rangle_{\Omega}^{-1} \langle l_n \cdot \mathbf{u}_h, e_r \rangle_{\Omega} \hat{q}_r = 0 \quad \forall e_i \in \mathcal{Q}_h, \quad (11)$$

where both sides of (7) have been pre-multiplied by the \mathcal{Q}_h mass matrix, $\mathbf{M} = \langle e_i, e_j \rangle_{\Omega}$. This equation conserves mass due to the telescopic property of the incidence matrix, $\mathbf{1}^T \mathbf{E} = 0$ [13].

Notably, (11) is the adjoint of the material form of the advection equation,

$$\dot{q} + \mathbf{u} \cdot \nabla q = 0, \quad (12)$$

which is given discretely (assuming periodic boundary conditions) as

$$\langle e_i, e_j \rangle_{\Omega} \hat{q}_j - \langle e_i, \mathbf{u}_h \cdot l_k \rangle_{\Omega} \langle l_m, l_k \rangle_{\Omega}^{-1} \mathbf{E}_{nm}^T \langle e_n, e_r \rangle_{\Omega} \hat{q}_r = 0 \quad \forall e_i \in \mathcal{Q}_h, \quad (13)$$

since the advection operator in (11),

$$\mathbf{A} = \langle e_i, e_k \rangle_{\Omega} \mathbf{E}_{km} \langle l_n, l_m \rangle_{\Omega}^{-1} \langle l_n \cdot \mathbf{u}_h, e_r \rangle_{\Omega}, \quad (14)$$

and the corresponding operator in (13),

$$\mathbf{B} = -\langle e_i, \mathbf{u}_h \cdot l_k \rangle_{\Omega} \langle l_m, l_k \rangle_{\Omega}^{-1} \mathbf{E}_{nm}^T \langle e_n, e_r \rangle_{\Omega}, \quad (15)$$

are related as $\mathbf{B} = -\mathbf{A}^T$.

As for other discretisations [14, 15], the adjoint property for the flux form and material form advection operators allows for exact energy conservation for incompressible flows ($\mathbf{E} \mathbf{u}_h = 0$). This is achieved via a skew-symmetric form of the advection operator as

$$\mathbf{S} = \frac{1}{2}(\mathbf{A} + \mathbf{B}) = \frac{1}{2}(\mathbf{A} - \mathbf{A}^T), \quad (16)$$

and a centered time integration scheme of the form

$$\mathbf{M} \frac{(\hat{q}_h^{n+1} - \hat{q}_h^n)}{\Delta t} + \mathbf{S} \frac{(\hat{q}_h^{n+1} + \hat{q}_h^n)}{2} = 0. \quad (17)$$

Pre-multiplying both sides of (17) by $(\hat{q}_h^{n+1} + \hat{q}_h^n)/2$ gives the conservation of energy as

$$\hat{q}_h^{n+1} \mathbf{M} \hat{q}_h^{n+1} = \hat{q}_h^n \mathbf{M} \hat{q}_h^n, \quad (18)$$

due to the skew-symmetry of \mathbf{S} and the bi-linearity of \mathbf{M} .

2. Petrov-Galerkin flux upwinding

The advection operators described in the preceeding section have numerous appealing properties, including high order error convergence (for smooth solutions), mass and energy conservation, and purely imaginary eigenvalues (strict hyperbolicity). However they are also prone to spurious oscillations in the presence of sharp, poorly resolved gradients. In this section we describe modified formulations which smooth out these oscillations via upwinding. A consequence of this upwinding construction is that the eigenvalues of the operators are no longer purely hyperbolic, such that non-zero real eigenvalues are present that act to damp the solutions.

In order to upwind the mass flux test functions, we may equivalently evaluate these at *downstream* locations [9], defined locally as

$$\xi^d = \xi + \Delta t \int_{s=0}^1 J^{-1}(\xi) \mathbf{u}(x, s) ds, \quad (19)$$

where $J^{-1}(\xi)$ is the Jacobian matrix inverse, such that $l_i^u = l_i(\xi^d)$. The mass flux is then computed using a Petrov-Galerkin formulation as

$$\langle l_i^u, l_j \rangle_{\Omega} \hat{F}_j^{PG} = \langle l_i^u \cdot \mathbf{u}_h, e_k \rangle_{\Omega} \hat{q}_k, \quad \forall l_i^u \in \mathcal{U}_h. \quad (20)$$

Since the trial space remains unaltered, the resulting mass flux \hat{F}_j^{PG} maintains its compatible mapping with respect to the space of the tracer field, \mathcal{Q}_h . The Petrov-Galerkin upwinded advection operator is then given as

$$\mathbf{A}_{PG;\Delta t} = \langle e_i, e_k \rangle_{\Omega} \mathbf{E}_{km} \langle l_n^u, l_m \rangle_{\Omega}^{-1} \langle l_n^u \cdot \mathbf{u}_h, e_r \rangle_{\Omega}. \quad (21)$$

The corresponding material form advection operator is given as

$$\mathbf{B}_{PG;\Delta t} = -\mathbf{A}_{PG;\Delta t}^T = -\langle e_i, \mathbf{u}_h \cdot l_k^d \rangle_{\Omega} \langle l_m, l_k^d \rangle_{\Omega}^{-1} \mathbf{E}_{nm}^T \langle e_n, e_r \rangle_{\Omega} \quad (22)$$

where $l_i^d = l_i(\xi^u)$ and

$$\xi^u = \xi - \Delta t \int_{s=0}^1 J^{-1}(\xi) \mathbf{u}(x, s) ds. \quad (23)$$

Note that in each of the examples presented in this article we use a simple first order Euler integration in order to determine ξ^d and ξ^u .

3. Results

We first verify the error convergence properties for the upwinded mass flux, for a manufactured solution of the form $q = 0.5(1.0 - \cos(2\pi x))$, $\mathbf{u} = 0.4 + 0.2(1.0 + \sin(2\pi x))$ over a periodic domain of unit length $L = 1$, such that $x \in [0, L)$, and compare the convergence rates against the original definition of the discrete mass flux for $\mathbf{F} = \mathbf{u}q$. Note that this corresponds to a compressible velocity field, and so the material form advection operator is not a valid adjoint. For this test we compare two configurations, the first for elements of degree $p = 3$, and the second for elements of degree $p = 6$. In both cases we use $n_e = 4 \times n^2$ elements, for $n = 1, 2, 3, 4, 5$ and a time step of $\Delta t = 0.0625/n_e$ in order to upwind the trial functions for the Petrov-Galerkin formulation. As observed in Fig. 1, both the original and upwinded mass fluxes converge at their theoretical rates for both $p = 3$ and $p = 6$ within the $L^2(\Omega)$ norm. The convergence is marginally better for the upwinded formulation, however this improvement diminishes with polynomial order.

As a second test we time step the advection equation using the original, upwinded flux form, and downwinded material form advection operators for an incompressible flow of $\mathbf{u} = 0.4$ and an initial tracer distribution of

$$q(x, 0) = \begin{cases} 0.5 + 0.5 \tanh(200(x - 0.4)), & x < 0.5 \\ 0.5 + 0.5 \tanh(200(0.6 - x)), & x \geq 0.5 \end{cases} \quad (24)$$

over the unit domain of $L = 1$ with 20 elements and a time step of $\Delta t = 0.005$ over a single revolution of period $T = 2.5$. In each case a second order centered time stepping scheme of the form

$$\mathbf{M} \frac{(\hat{q}_h^{n+1} - \hat{q}_h^n)}{\Delta t} + \mathbf{A} \frac{(\hat{q}_h^{n+1} + \hat{q}_h^n)}{2} = 0 \quad (25)$$

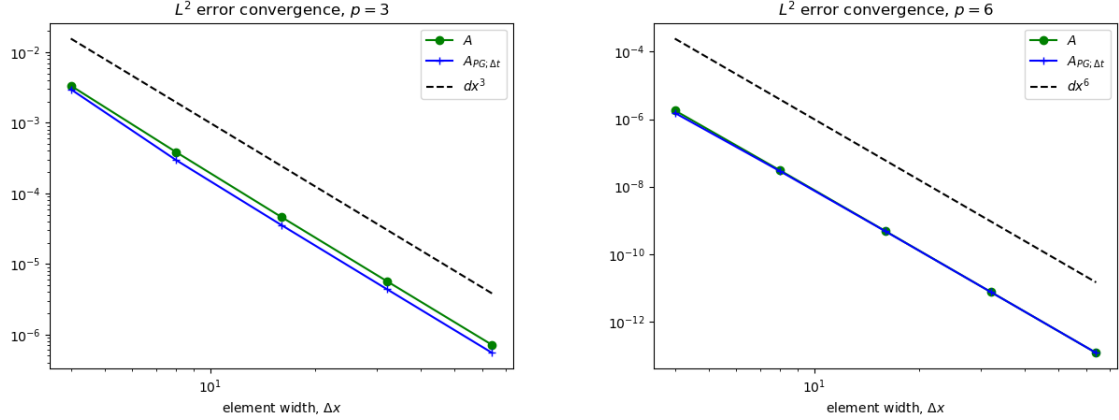


Figure 1: Mass flux error convergence for $p = 3$ (left) and $p = 6$ (right).

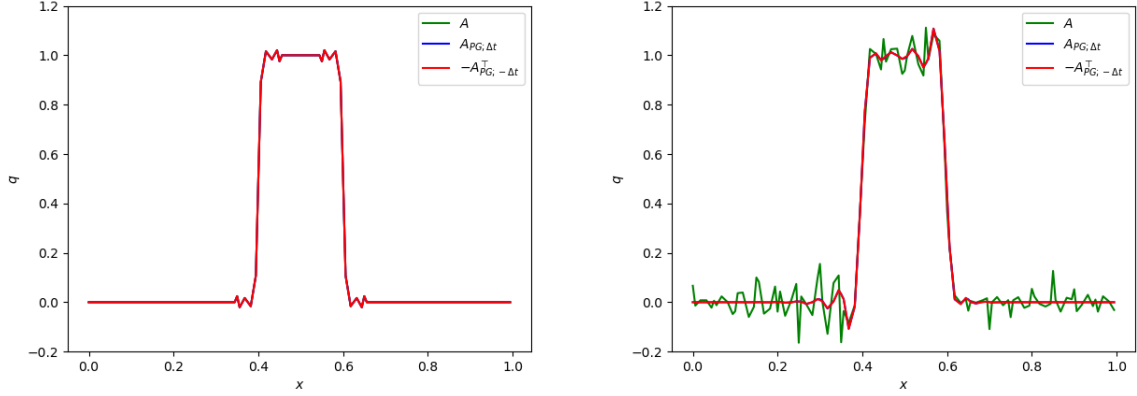


Figure 2: Initial state (left) and final state (right) after one revolution, $p = 5$, 20 elements, $u = 0.4$, $\Delta t = 0.005$.

was employed (with \mathbf{A} replaced with $\mathbf{A}_{PG,\Delta t}$ and $-\mathbf{A}_{PG,-\Delta t}^T$ for the upwinded flux form and downwinded material forms respectively).

Figure 2 shows the initial and final results for the advection test. The upwinded test function flux form and downwinded trial function material form solutions are indistinguishable, however both are markedly less oscillatory than the original solution. The corresponding mass and energy conservation errors are given in Fig. 3. While all three operators preserve mass conservation to machine precision, the Petrov-Galerkin operators dissipate energy, while these energy conservation errors remain bounded for the original operator.

Figures 4 and 5 show the imaginary and real components of the dispersion relations for the advection operators of degree $p = 3$ and $p = 6$ respectively with 40 elements and a time step of $\Delta t = 0.005$. These are computed by first interpolating the eigenvectors from the Q_h space to physical space, and then projecting these physical space solutions onto Fourier modes (for details see the appendix).

The imaginary eigenvalues of the Petrov-Galerkin operators are closer to the analytic, dispersionless solution of $\omega = k$ (indicated by the solid black lines in Figs. 4 and 5). Notably the Petrov-Galerkin operators also seal up the spectral gaps which are characteristic of both collocated [16] and mixed [17] high order finite element discretisations. This behaviour has also been observed for hyperviscosity in the context of collocated spectral elements [18]. However while the real eigenvalues are at machine precision for the original operator, indicating purely hyperbolic advection, these are non-zero for the Petrov-Galerkin formulations, indicating dissipative solutions biased towards higher wave

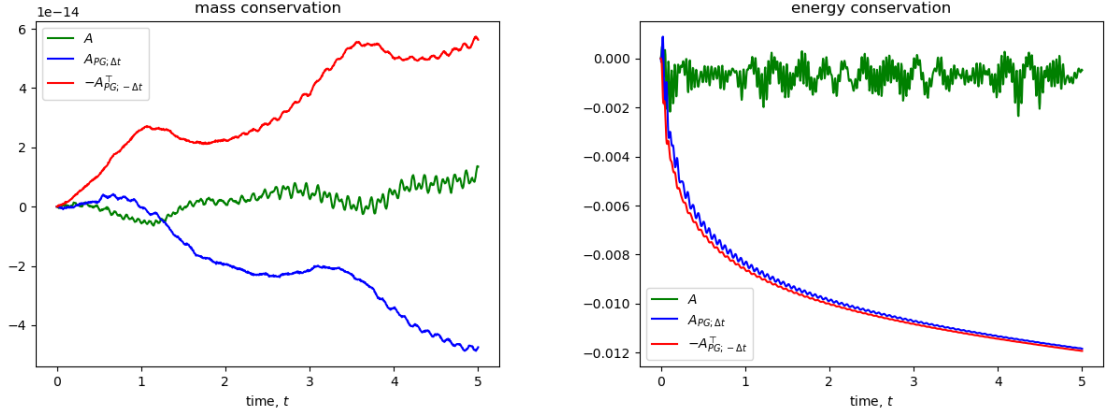


Figure 3: Mass (left) and energy (right) conservation errors with time, $p = 5$, 20 elements, $u = 0.4$, $\Delta t = 0.005$.

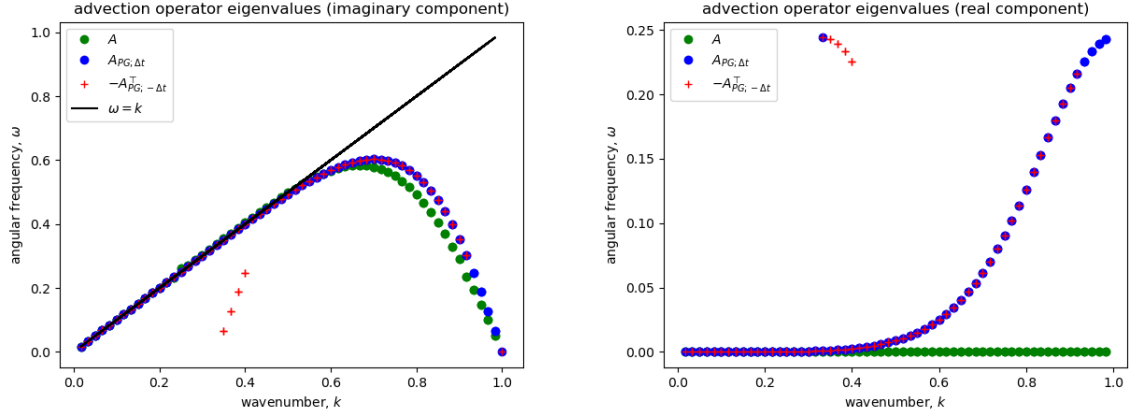


Figure 4: Imaginary (left) and real (right) eigenvalues for the advection operators, 40 elements, $p = 3$, $u = 0.4$, $\Delta t = 0.005$.

numbers. The dissipation profile of these operators steepens with polynomial degree, in analogy to a higher power viscosity operator.

Figure 6 plots the real component of the eigenvalues, ω^r against the imaginary, ω^i for the centered advection operator $(\mathbf{M} + 0.5\Delta t\mathbf{A})^{-1}(\mathbf{M} - 0.5\Delta t\mathbf{A})$ (and similarly for $\mathbf{A}_{PG;\Delta t}$ and $-\mathbf{A}_{PG;\Delta t}^T$), as given in (25), for a time step of $\Delta t = 0.005$. The original operator eigenvalues sit on the unit circle, indicating the neutral stability of this formulation. This is also reflected in the bounded energy conservation errors, as shown in Fig. 3. The dissipative nature of the Petrov-Galerkin operators is reflected in the fact that the eigenvalues for the time integration operator sit *inside* the unit circle.

As for the original operator, both forms of the Petrov Galerkin advection operator may be used to construct skew-symmetric formulations, as given in (16). In each case, energy is conserved to machine precision as shown in Fig. 7. However this is a direct result of the cancellation of the upwinding contributions of the Petrov-Galerkin operators such that the solutions are once again oscillatory and there is no discernible benefit to the use of these formulations over the original operator.

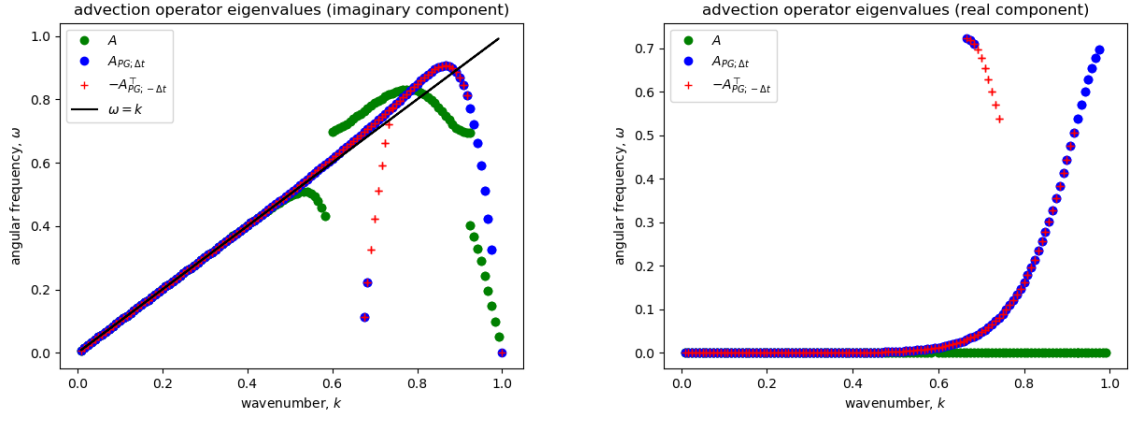


Figure 5: Imaginary (left) and real (right) eigenvalues for the advection operators, 40 elements, $p = 6$, $u = 0.4$, $\Delta t = 0.005$.

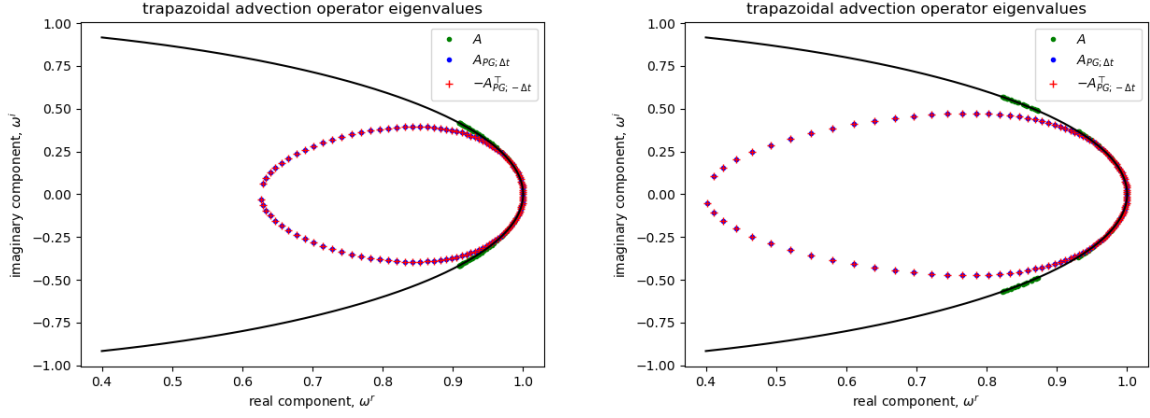


Figure 6: Centered space time advection operator eigenvalues (real), $p = 3$, 40 elements (left), and $p = 6$, 20 elements (right), $u = 0.4$, $\Delta t = 0.005$. The black line indicates the unit circle.

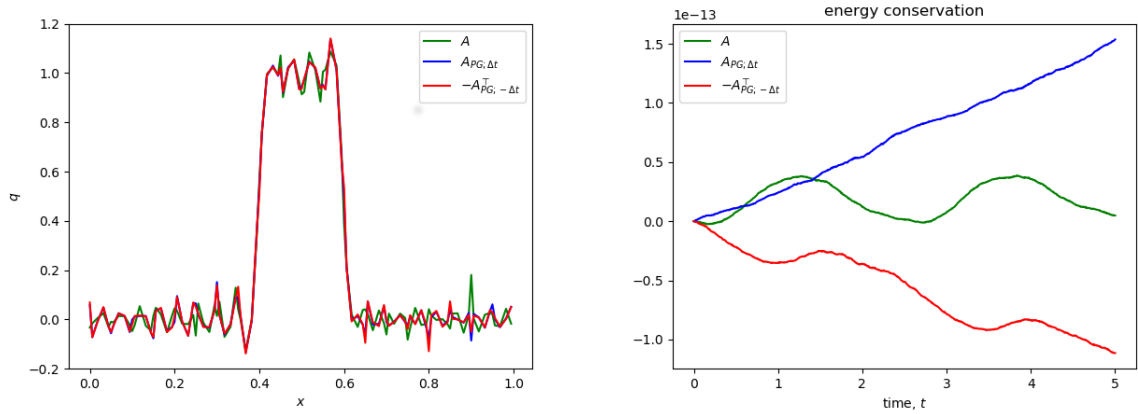


Figure 7: Skew-symmetric formulation: final state after one revolution (left) and energy conservation errors (right), $p = 5$, 20 elements, $u = 0.4$, $\Delta t = 0.005$.

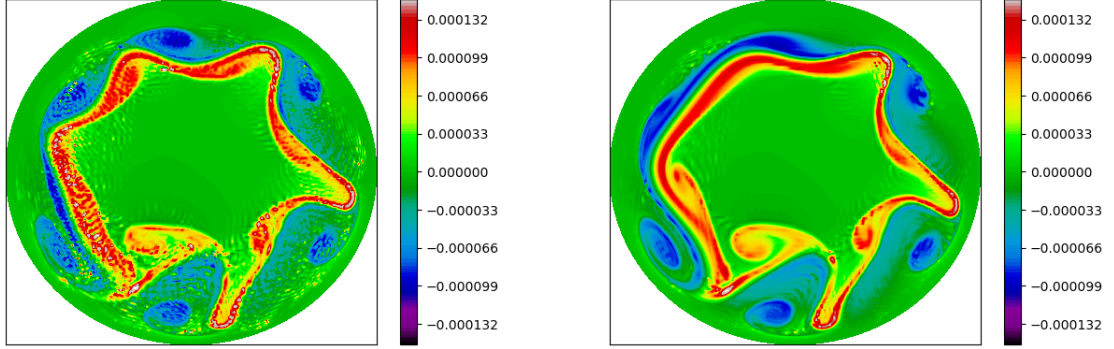


Figure 8: Vorticity field for the Galewsky test case (day 6); left: original formulation, right: Petrov-Galerkin upwinded vorticity.

4. Application to vorticity stabilisation in shallow water on the sphere

In order to demonstrate the usefulness of the Petrov Galerkin upwinded formulations described above this is applied to the diagnosis and interpolation of the vorticity for the rotating shallow water equations on the sphere. The model uses a mixed mimetic spectral element spatial discretisation on a cubed sphere [11] for which the vorticity, velocity and fluid depth are discretised on the $W \subset H(\text{rot}, \Omega)$, $U \subset H(\text{div}, \Omega)$ and $Q \subset L^2(\Omega)$ spaces respectively, and a semi-implicit time integration scheme that allows for the exact balance of energy exchanges [6]. The model conserves mass, vorticity and energy in space and time.

No dissipation is applied to the model, except that in the second simulation the upwinded stabilisation is applied by sampling the vorticity field trial functions at downstream locations in a two dimensional analogue of (22). The vorticity field is diagnosed in the discrete weak form analogue of $\omega = \nabla \times \mathbf{u}$. Borrowing from the notation in [11] this is given as

$$\langle \epsilon_i^W, \epsilon_j^{W,d} \rangle_{\Omega} \omega_j^d = -(\mathbf{E}_{k,j}^{1,0})^\top \langle \tilde{\epsilon}_k^U, \tilde{\epsilon}_l^U \rangle_{\Omega} u_l, \quad \forall \epsilon_i^W \in W, \quad (26)$$

where $\epsilon_j^{W,d} \in W$ are the set of downwinded trial functions and $(\mathbf{E}_{k,j}^{1,0})^\top$ is the discrete approximation of the *curl* operator in the weak form. The upwinded vorticity is then coupled to the prognostic equations through the vector invariant form of the momentum equation $\dot{\mathbf{u}} = -(\omega + f) \times \mathbf{u} + \dots$ (where f denotes the Coriolis term) [11] as

$$\langle \tilde{\epsilon}_i^U, \tilde{\epsilon}_j^U \rangle_{\Omega} u_j^{n+1} = \langle \tilde{\epsilon}_i^U, \tilde{\epsilon}_j^U \rangle_{\Omega} u_j^n - \Delta t \langle \tilde{\epsilon}_i^U, (\bar{\omega}_h^d + f_h) \times \tilde{\epsilon}_l^U \rangle_{\Omega} \bar{u}_l + \dots, \quad \forall \tilde{\epsilon}_i^U \in U, \quad (27)$$

where

$$\bar{\omega}_h^d = \frac{1}{2} \sum_i \left(\epsilon_i^{W,d,n} \omega_i^{d,n} + \epsilon_i^{W,d,n+1} \omega_i^{d,n+1} \right) \quad (28)$$

is a time centered approximation to the upwinded vorticity, ω_h^d .

The discrete vorticity space, W is composed as a two dimensional tensor product of nodal bases (4), and as such the upwind stabilisation of this space is achieved through the downstream sampling of the trial functions in both dimensions. Since the vorticity, $\omega_h \in W$ does not project onto the energy space, Q [11, 13], the upwinding modification of the vorticity does not affect the conservation properties of the model. While the upwinding of the vorticity does dissipate potential enstrophy, this is not conserved in the original formulation due to the use of inexact quadrature [13]. This upwinded vorticity formulation is conceptually similar to the anticipated potential vorticity method [19], which similarly stabilises the vorticity by dissipating enstrophy. Note that this vorticity stabilisation does not address nonlinearities associated with the oscillation of gravity waves, which may still yield aliasing errors.

The code was configured according to a standard test case for rotating shallow water on the sphere [20], which is initialised as a steady jet overlaid with a small perturbation of the height field. Over several days this acts to destabilise the jet into a series of barotropic eddies. In each case the model was run with 32 elements of degree $p = 3$ on each

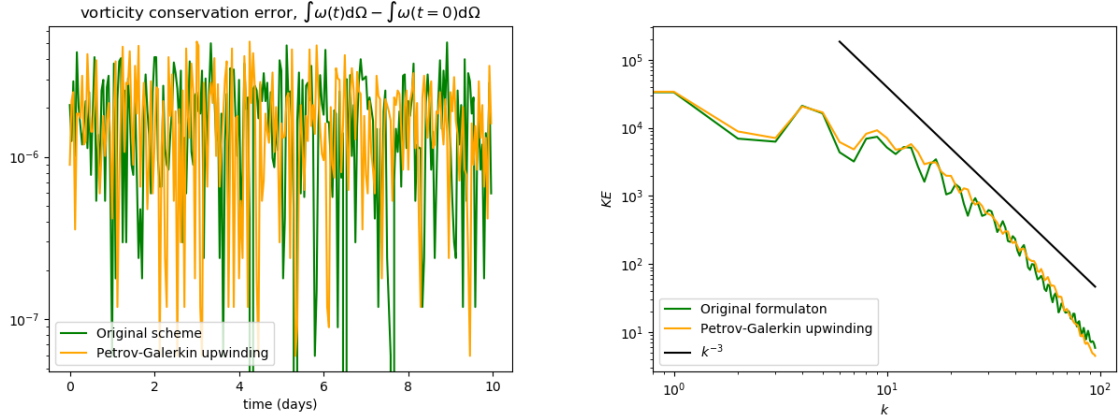


Figure 9: Vorticity conservation errors (un-normalised) for the original and upwinded formulations (left), and kinetic energy power spectra at day 6 (right).

face of the cubed sphere and a time step of $\Delta t = 300$ s. Note that this time step is well outside the stability region of an explicit time integrator at this spatial resolution. As observed in Fig. 8, the Petrov-Galerkin upwinding of the vorticity diagnostic equation leads to a more coherent solution, with fewer aliasing errors.

Figure 9 shows the vorticity conservation errors integrated over the sphere (with radius 6,371,220.0m). These are un-normalised, since the total vorticity integrates to zero. There is no perceivable difference in the errors between the two schemes, and these are consistent with previous results [11]. This figure also shows the kinetic energy spectra of the two schemes at day 6. These are computed by first interpolating the kinetic energy onto a regular latitude–longitude grid, and then decomposing this solution into spherical harmonics. Both schemes exhibit an upscale cascade of k^{-3} , consistent with the theory of two dimensional turbulence, however the upwinded scheme shows less oscillation in this cascade, reflecting the minimisation of aliasing errors.

5. Conclusions

This article describes the formulation of upwinded advection operators for mixed mimetic spectral elements in both flux form and material form. These operators exhibit dissipation of high wave numbers which suppresses spurious high frequency oscillations for sharp, poorly resolved gradients. The dissipation profiles increase with polynomial degree in a way that reflects the profile of higher order viscosity terms. These upwinded formulations are relatively simple to compute and cheap to assemble. However by evaluating oscillatory basis functions outside of the canonical domain they increase the condition number of the matrices necessary to determine mass fluxes and tracer gradients. Also for nodal bases which are orthogonal with respect to the standard Gauss-Lobatto-Legendre quadrature points, by moving these quadrature point locations this orthogonality is broken such that the corresponding mass matrices are no longer diagonal.

This upwinding formulation has been coupled to an existing solver for the shallow water equations on the sphere, where it is shown to reduce aliasing errors, as well as to improve the turbulence profile. In future work the application of this scheme to the stabilisation of temperature fluxes for the compressible Euler equations will be investigated.

Appendix: computation of eigenvalues

Assuming exact time integration, the semi-discrete advection equation is expressed as

$$\mathbf{M}^{-1} \mathbf{A} q_h = \omega q_h \quad (29)$$

for $q_h(x, t) = q_h(x) e^{-\omega t}$. The eigenvalues, ω_h and eigenvectors, v_h of this square operator may be computed using any standard eigenvalue solver as $\omega_h, v_h = \text{eig}(\mathbf{M}^{-1} \mathbf{A})$ (and similarly for $\mathbf{A}_{PG;\Delta t}$ and $-\mathbf{A}_{PG;-\Delta t}^T$). We then define two

additional operators, an interpolation operator between degrees of freedom in Q_h and physical coordinates,

$$\mathbf{Q}, \quad Q_{jk} := e_k(\xi_j) \quad (30)$$

(for which the Jacobian terms cancel), and a Fourier interpolation operator,

$$\mathbf{F}, \quad F_{jk} := \cos(2\pi k x_j / L) + i \sin(2\pi k x_j / L) \quad (31)$$

where L is the domain length, i denotes the imaginary number, and k a given Fourier mode. Each eigenvector, v_h is then projected onto a vector v_h^f representing an expansion over Fourier modes as

$$v_h^f = \mathbf{F}^{-1} \mathbf{Q} v_h. \quad (32)$$

We then sort v_h^f in order to determine the Fourier mode with the largest amplitude, k_h . This mode is then paired with the original eigenvalue, ω_h in order to construct the dispersion relation.

6. Acknowledgments

David Lee would like to thank Dr. Darren Engwirda for the idea of applying the Petrov-Galerkin scheme to the problem of vorticity advection in geophysical flows. This project was supported by resources and expertise provided by CSIRO IMT Scientific Computing.

References

- [1] A. N. Brooks, T. J. R. Hughes, Streamline upwind/Petrov-Galerkin formulations for convection dominated flows with particular emphasis on the incompressible Navier-Stokes equations, *Comput. Meth. Appl. Mech. Engrg.* 32 (1982) 199–259
- [2] T. J. R. Hughes, G. R. Feijoo, L. Mazzei, J.-B. Quincy, The variational multiscale method—a paradigm for computational mechanics, *Comput. Methods Appl. Mech. Engrg.* 166 (1998) 3–24
- [3] S. Marras, J. F. Kelly, F. X. Giraldo, M. Vázquez, Variational multiscale stabilization of high-order spectral elements for the advection-diffusion equation, *J. Comput. Phys.* 231 (2012) 7187–7213
- [4] M. Gerritsma, Edge functions for spectral element methods, in: *Spectral and high order methods for partial differential equations*, Lecture Notes in Computational Science and Engineering, Springer 76 (2011) 199–207
- [5] J. Kreeft, M. Gerritsma, Mixed mimetic spectral element method for Stokes flow: A pointwise divergence-free solution, *J. Comp. Phys.* 240 (2013) 284–309.
- [6] G. A. Wimmer, C. J. Cotter, W. Bauer, Energy conserving upwinded compatible finite element schemes for the rotating shallow water equations, *J. Comput. Phys.* 401 (2020) 109016
- [7] T. F. Russell, M. A. Celia, An overview of research on Eulerian-Lagrangian localised adjoint methods (ELLAM), *Adv. Water Resour.* 25 (2002) 1215–1231
- [8] W. Guo, R. D. Nair, J.-M. Qiu, A conservative semi-Lagrangian discontinuous Galerkin scheme on the cubed sphere, *Mon. Wea. Rev.* 142 (2014) 457–475
- [9] D. Lee, R. Lowrie, M. Petersen, T. Ringler, M. Hecht, A high order characteristic discontinuous Galerkin scheme for advection on unstructured meshes, *J. Comput. Phys.* 324 (2016) 289–302
- [10] P. A. Bosler, A. M. Bradley, M. A. Taylor, Conservative Multimoment Transport along Characteristics for Discontinuous Galerkin Methods, *SIAM J. Sci. Comput.* 41(4) (2019) B870–B902
- [11] D. Lee, A. Palha, A Mixed mimetic spectral element model of the rotating shallow water equations on the cubed sphere, *J. Comput. Phys.* 375 (2018) 240–262
- [12] A. Palha, P. P. Rebelo, M. Gerritsma, Mimetic spectral element advection, *Spectral and High Order Methods for Partial Differential Equations ICOSAHOM 2012*, Lecture Notes in Computational Science and Engineering, 95, Springer International Publishing (2014) 325–335
- [13] D. Lee, A. Palha, M. Gerritsma, Discrete conservation properties for shallow water flows using mixed mimetic spectral elements, *J. Comput. Phys.* 357 (2018) 282–304
- [14] Y. Morinishi, Skew-symmetric form of convective terms and fully conservative finite difference schemes for variable density low-Mach number flows, *J. Comput. Phys.* 229 (2010) 276–300
- [15] A. Palha, M. Gerritsma, A mass, energy, enstrophy and vorticity conserving (MEEVC) mimetic spectral element discretization for the 2D incompressible Navier-Stokes equations, *J. Comput. Phys.* 328 (2017) 200–220
- [16] T. Melvin, A. Staniforth, J. Thuburn, Dispersion analysis of the spectral element method, *Q. J. R. Meteorol. Soc.* 138 (2012) 1934–1947
- [17] C. Eldred, D. Y. Le Roux, Dispersion analysis of compatible Galerkin schemes for the 1D shallow water model, *J. Comput. Phys.* 371 (2018) 779–800
- [18] P. A. Ullrich, D. R. Reynolds, J. E. Guerra, M. A. Taylor, Impact and importance of hyperdiffusion on the spectral element method: A linear dispersion analysis, *J. Comput. Phys.* 375 (2018) 427–446
- [19] R. Sadourny, C. Basdevant, Parameterization of Subgrid Scale Barotropic and Baroclinic Eddies in Quasi-geostrophic Models: Anticipated Potential Vorticity Method, *J. Atmos. Sci.* 42 (1985) 1353–1363
- [20] J. Galewsky, R. K. Scott, L. M. Polvani, An initial-value problem for testing numerical models of the global shallow water equations, *Tellus* 56A (2004) 429–440